RSC Advances

PAPER

View Article Online
View Journal | View Issue

Cite this: *RSC Adv.*, 2024, **14**, 35743

Preparation and antioxidant properties of tannic acid/copper ion nanozyme hybrid nanofibrous membranes†

Qiao Wu, Jingshu Xiao, Hu Zhuang, Fenghai Zhao, Ruoxi Li and Duntie Zhang*

Received 22nd July 2024
Accepted 1st November 2024

DOI: 10.1039/d4ra05314a

rsc.li/rsc-advances

Excess free radicals can have some negative effects on human health. In this paper, a nanozyme was successfully constructed by the coordination of copper ions and tannic acid, and its structure and elemental distribution were determined by Fourier transform infrared spectroscopy, scanning electron microscopy and X-ray photoelectron spectroscopy. Free radical scavenging experiments confirmed that it possessed superoxide dismutase-like activity, catalase-like activity, and hydroxyl radical scavenging ability. The results of thermogravimetric analysis experiments demonstrated that it possessed good thermal stability. A polyacrylonitrile hybrid nanofibrous membrane loaded with Cu/TA nanozyme was successfully constructed by electrospinning technology, and the maximum scavenging rate of DPPH and ABTS radicals can reach 64.22% and 58.44%, respectively. The nanofiber membrane also exhibited the ability to protect cells from oxidative stress damage. Therefore, the hybrid nanofibrous membrane has a broad application prospect in fields such as food preservation and biomedicine.

1 Introduction

In living organisms, free radicals are usually considered as harmful substances and an important factor contributing to aging.[1,2] Free radicals can be classified as endogenous and exogenous. In eukaryotic cells, endogenous free radicals are mostly produced by mitochondria.[3] Electrons leaked from the mitochondrial respiratory chain react with O_2 to generate superoxide radical ($^{\bullet}O_2^-$), which can be further converted to hydrogen peroxide (H_2O_2) and hydroxyl radical ($^{\bullet}OH$).[4,5] Exogenous free radicals can be attributed to various external stimuli such as ultraviolet light, air/water pollution and toxic chemicals.[6] Harmful free radicals are responsible for tissue damage and various diseases including cancer, neurodegenerative diseases, diabetes and cardiovascular diseases.[7–11] Therefore, the design and fabrication of functional materials with antioxidant activity has become an important approach to scavenge free radicals and protect the host from damage.

Currently, antioxidants are mainly divided into natural antioxidants and synthetic antioxidants. Antioxidant enzymes synthesized *in vivo* are critical parts of the antioxidant defense network.[12] Superoxide dismutase (SOD), catalase and glutathione peroxidase eliminate excess free radicals in the organism to maintain homeostasis.[13] Leaves, fruits and seeds of plants are the main sources of antioxidants.[14] Natural antioxidants mainly contain polyphenolic compounds, vitamins and carotenoids with a wide range of biological activities and rich nutritional value. Synthetic compounds, including nitrones/nitroxides, iron ion chelators and thiols, have also been widely used for scavenging free radicals.[15–17] Generally, synthetic antioxidants are more active and pure than natural antioxidants and have constant antioxidant activity, but their toxicity and safety are widely concerned.[18]

Nanomaterials have great potential in the field of developing novel antioxidants. Some nanomaterials, such as metal and metal oxide-based nanoparticles, exhibit free radical trapping and/or SOD-like and catalase-like activities with excellent scavenging ability of free radicals.[11,19] Compared to natural enzymes, such nanomaterials exhibit tunable activity, higher stability and tolerance to harsh environments.[20,21] In recent years, nanomaterials with enzyme-like activity (nanozymes) have shown promise as substitutes for natural enzymes. Many natural enzymes are metal-based enzymes and their metal catalytic activity centers are mainly copper, iron or zinc ions. Among them, copper is the active center of many proteins and enzymes and plays a crucial role in the function of several enzymes, including tyrosinase and copper zinc superoxide dismutase (SOD1).[13,22,23] Therefore, it is reasonable to use copper ions to prepare nanozymes for free radical scavenging.

Inspired by antioxidant enzymes, Cu/TA nanozyme with antioxidant activity were constructed in this study by self-assembly of copper ions and tannic acid (TA). The natural active ingredient TA, which is widely found as a water-soluble polyphenol in the barks and fruits of many plants with anti-inflammatory, antioxidant, and anti-microbial properties, was used as the reaction material.[24,25] In addition, TA can chelate

China Tobacco Hubei Industrial LLC, Wuhan, Hubei, 430072, China

† Electronic supplementary information (ESI) available. See DOI: https://doi.org/10.1039/d4ra05314a

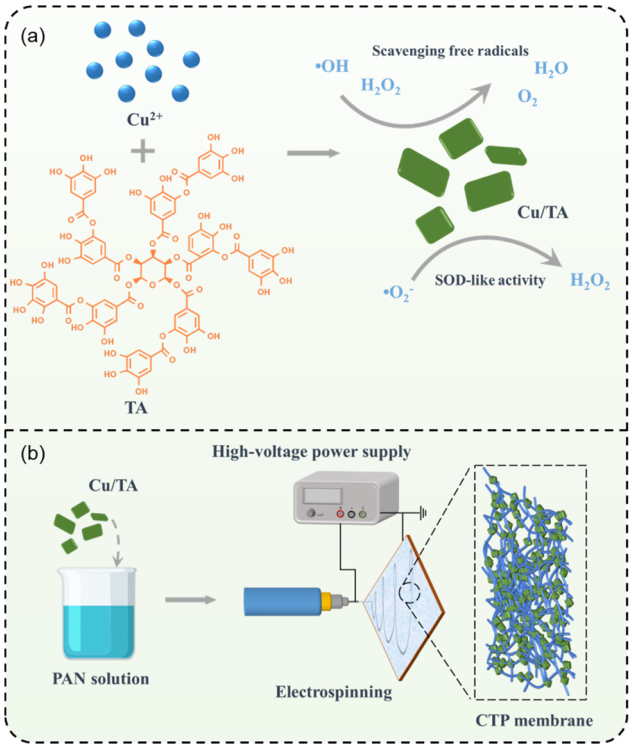

Fig. 1 Schematic diagram of the preparation process of (a) Cu/TA nanozyme and (b) CTP nanofibrous membranes.

a variety of metal ions through coordination bonds and rapidly form stable five-element ring complexes with these ions.[13,26] Although the preparation of nanoparticles using copper ions and TA has been reported in the literature,[27–29] the Cu/TA nanosheet in this work were prepared by a green one-pot method. This simple synthesis process and mild reaction conditions provide an effective method for the preparation of Cu/TA nanozyme at low-cost and large-scale production. The obtained Cu/TA nanozyme combine the advantages of nanozyme and natural antioxidant, thus achieving multiple free radical scavenging abilities with the assistance of TA.[30] The results showed that the Cu/TA nanozymes possessed SOD-like activity and could effectively remove $^{\bullet}O_2^-$. In addition, Cu/TA nanozymes exhibited excellent catalase-like activity and the ability to scavenge $^{\bullet}OH$ (Fig. 1a). This synergistic antioxidant activity allows it to act as an effective antioxidant for scavenging various free radicals. In addition, the unique coordination structure endows the Cu/TA nanozyme with excellent thermal stability. The Cu/TA nanozymes were further loaded into polyacrylonitrile (PAN) nanofibrous membranes by electrospinning (Fig. 1b), and the prepared Cu/TA-PAN hybrid nanofibrous membranes (CTP membranes) exhibited good biocompatibility and antioxidant activity, which is promising for the application in the fields, such as food preservation and biomedicine.[25,31,32]

2 Materials and methods

2.1 Materials

Tannic acid (TA) was provided by Shanghai Macklin Biochemical Technology Co., Ltd. Polyacrylonitrile (PAN, Mw = 150 000) was purchased from DuPont. 3,3′,5,5′-tetramethyl-benzidine (TMB), 1,1-diphenyl-2-trinitrophenylhydrazine (DPPH), 2,2′-azino-bis(3-ethylbenzthiazoline-6-sulphonate) (ABTS) and NaAc-HAc buffer (pH = 3.6) were purchased from Shanghai yuanye Bio-Technology Co., Ltd. Hydroxyl free radical assay kit (A018-1-1) and inhibition and produce superoxide anion assay kit (A052-1-1) were provided by Nanjing Jiancheng Bioengineering Institute. Copper(II) chloride dihydrate ($CuCl_2 \cdot 2H_2O$), potassium persulfate ($K_2S_2O_8$), *N*,*N*-dimethylformamide (DMF), hydrogen peroxide (H_2O_2, 30%) and anhydrous ethanol were purchased from Sinopharm Chemical Reagent Co., Ltd. All chemical reagents were of analytical grade and used as received without further purification.

2.2 Preparation of Cu/TA nanozyme

According to the method reported in the literature,[33] Cu/TA nanozyme was synthesized through the chelation reaction between Cu^{2+} and TA. Briefly, 0.025 g of TA and 0.875 g of $CuCl_2$ were separately dissolved in 25 mL of ultrapure water. The two solutions were then mixed and adjusted to pH 7.4 using 2 M NaOH solution. The reaction mixture was stirred at room temperature for 3 h. The obtained precipitate was collected by centrifugation at 8000 rpm, washed three times with ultrapure water, and freeze-dried. The obtained Cu/TA nanozyme was stored at 4 °C.

2.3 Characterization of Cu/TA nanozyme

2.3.1 Fourier transform infrared spectroscopy (FT-IR). Functional group analysis of Cu/TA nanozyme was carried out using FT-IR (icolet iS10, Thermofisher). All samples were freeze-dried before experimenting. Samples were mixed with potassium bromide, ground, and pressed into pellets. The FT-IR spectra were collected in the range of 500–4000 cm^{-1}.

2.3.2 Dynamic light scattering (DLS). Before analysis, Cu/TA nanozyme and TA powder were redispersed in distilled water at a concentration of 800 μg mL^{-1}. DLS measurements were performed using the Malvern Nano ZS analyzer to determine the hydrodynamic diameter, polydispersity index (PDI), and zeta potential of Cu/TA nanozyme.

2.3.3 Field emission scanning electron microscopy (FE-SEM). The size and morphology of the Cu/TA nanozyme were characterized by FE-SEM (SU8010, Hitachi). Before observation, the Cu/TA nanozyme was placed on double-sided carbon tape and sputtered with gold. Energy dispersive spectroscopy (EDS) was used for elemental analysis.

2.3.4 X-ray photoelectron spectroscopy (XPS). XPS spectra were collected in the Kratos AXIS Supra+ XPS microscope using monochromatic Al Kα radiation, and the XPS spectra were deconvoluted using CasaXPS software.

2.3.5 Thermogravimetric analysis (TGA). TGA curves of TA and Cu/TA nanozyme were recorded using the Mettler Toledo TGA/DSC 3+ analyzer in nitrogen atmosphere (20 mL min^{-1}) from 30 to 600 °C at a heating rate of 10 °C min^{-1}.

2.4 Multienzyme-like activity of Cu/TA nanozyme

2.4.1 $^{\bullet}O_2^-$ scavenging assay. The $^{\bullet}O_2^-$ scavenging ability of Cu^{2+}, TA and Cu/TA nanozyme was determined using the

inhibition and produce superoxide anion assay kit. The scavenging efficiency was calculated as follows:

$$\text{Scavenging efficiency (\%)} = (1 - A_{\text{sample}}/A_{\text{control}}) \times 100\%$$

2.4.2 $^{\cdot}$OH scavenging assay. The $^{\cdot}$OH scavenging ability of Cu^{2+}, TA and Cu/TA nanozyme was determined using the hydroxyl free radical assay kit. The scavenging efficiency was calculated as follows:

$$\text{Scavenging efficiency (\%)} = (1 - A_{\text{sample}}/A_{\text{control}}) \times 100\%$$

2.4.3 H_2O_2 scavenging assay. Cu/TA nanozyme catalyzed the decomposition of H_2O_2 to produce H_2O and O_2. TA and Cu/TA nanozyme was added to 1 mL of H_2O_2 solution, and the production of bubbles was observed and photographed.

2.4.4 Peroxidase (POD)-like activity of Cu/TA nanozyme. The POD-like activity of Cu/TA nanozyme was evaluated by oxidizing TMB to oxTMB in NaAc-HAc buffer. Briefly, 60 μL of Cu/TA nanozyme solution (1 mg mL^{-1}) was added to 100 μL of TMB solution (10 mM) and 200 μL of H_2O_2 (10 mM) in 1640 μL NaAc-HAc buffer solution. After incubation for 20 min at room temperature, the spectra of the mixed solution were detected by Ultraviolet-visible (UV-vis) spectrophotometer.

2.5 Preparation of PAN nanofibrous membranes

2.5.1 Spinning solution preparation. A certain amount of PAN was added to 20 mL DMF solution. The mixture was stirred at 60 °C using a water bath magnetic stirrer to prepare PAN solutions with mass fractions of 4%, 6%, 8%, 10%, and 12%.

2.5.2 Membrane preparation. The spinning solution was transferred into a 5 mL sterile syringe (22 G needle) and the syringe was fixed onto a syringe pump. The needle was connected to the positive terminal of a high-voltage power supply, while the plate collector and syringe pump were grounded. The spinning solution was ejected from the syringe, passing through the electric field, and finally deposited onto an aluminum foil-covered plate collector. The electrospinning parameters were set as follows: voltage: 20 kV; needle-to-receiver distance: 15 cm; and spinning solution flow rates were set at 0.5 mL h^{-1}, 1 mL h^{-1}, and 1.5 mL h^{-1}, respectively. The collected nanofibrous membranes were dried in an oven at 80 °C for 24 h to remove residual organic solvents.

2.6 Preparation of CTP membranes

After determining the optimal concentration of the PAN solution and process parameters, Cu/TA nanozymes were added to the mixed solution at 0.5, 1, 1.5, and 2% of the PAN mass. The mixture was stirred at 60 °C until homogeneous. CTP nanofibrous membranes were then prepared using the same process parameters.

2.7 Morphology of nanofibrous membranes

The samples were cut from the nanofibrous membranes, and after the samples were sprayed with gold, the surface morphology of the membranes was observed using the JSM6390LV SEM (JEOL). The fiber diameters were analyzed using Image J software.

2.8 Free radical scavenging ability of nanofibrous membranes

2.8.1 DPPH radical scavenging assay. 3 mg of nanofibrous membrane was incubated with 1.5 mL 0.1 mM DPPH ethanol solution in the dark. The absorbance of the solution at 517 nm was measured using UV-vis spectrophotometer. The scavenging efficiency of DPPH$^{\cdot}$ by different nanofiber membranes was calculated using pure DPPH$^{\cdot}$ solution as a blank control group. The calculation formula was:

$$\text{Scavenging efficiency (\%)} = (1 - A_1/A_0) \times 100\%$$

where A_0 denotes the absorbance of DPPH$^{\cdot}$ solution and A_1 denotes the absorbance of DPPH$^{\cdot}$ solution after reaction with the sample.

2.8.2 ABTS radical scavenging assay. Referring to the method reported in the literature,[34] ABTS$^{\cdot+}$ was generated by the reaction of 7.4 mM ABTS solution with 2.6 mM $K_2S_2O_8$, and the mixture was left at room temperature for 24 h in the dark. The ABTS$^{\cdot+}$ solution was adjusted to an absorbance of 0.70 ± 0.02 at 734 nm with ultrapure water before use. 3 mg of nanofibrous membrane was mixed with 3 mL of ABTS$^{\cdot+}$ solution and incubated in the dark. The scavenging efficiency of ABTS radicals by different nanofiber membranes was calculated using ABTS$^{\cdot+}$ solution as a blank control group. The calculation formula was:

$$\text{Scavenging efficiency (\%)} = (1 - A_1/A_0) \times 100\%$$

where A_0 denotes the absorbance of ABTS$^{\cdot+}$ solution and A_1 denotes the absorbance of ABTS$^{\cdot+}$ solution after reaction with the sample.

2.9 *In vitro* cytocompatibility study

The *in vitro* cytocompatibility assay of nanofibrous membranes were conducted using the extract method. Mouse L929 fibroblast cells were cultured in HyClone™ Dulbecco's modified eagles' medium (DMEM) containing 10% fetal bovine serum and 1% penicillin-streptomycin. After sterilization with 75% ethanol solution, the nanofibrous membranes were soaked with complete medium (6 cm^2 mL^{-1}) for 24 h to make the extracts. The L929 cells were seeded at 10 000 cells per well in a 96-well plate and incubated for 24 h at 37 °C in a 5% CO_2 atmosphere. Then, the cell culture medium was replaced with different extracts and fresh medium was used as control. After incubation for 24 h, the cell viability was detected in using the Cell Counting Kit-8 (CCK-8) method.

2.10 *In vitro* oxidative stress assay

The protective effect of nanofibrous membranes on cells in H_2O_2 simulated oxidative stress microenvironment was

investigated. The L929 cells were seeded in a 96-well plate at a density of 10 000 cells per well and incubated for 24 h. Then, the culture medium was removed and the cells were treated with 100 μL of fresh culture medium containing 500 μM H_2O_2 and sterile nanofibrous membranes for 6 h. The cell viability was determined by CCK-8 assay.

3 Results and discussion

3.1 Synthesis and characterization of Cu/TA nanozymes

3.1.1 Structure and morphology of Cu/TA nanozymes. The coordination between Cu^{2+} and TA was confirmed using FT-IR and XPS (Fig. 2). The FT-IR spectra of TA and Cu/TA nanozyme were shown in Fig. 2a. For the FT-IR spectrum of TA, the absorption peak observed at 3347 cm^{-1} corresponded to the presence of –OH groups. The absorption peak at 1717 cm^{-1} indicated the presence of C=O groups, and the absorption peaks at 1613 cm^{-1} and 1537 cm^{-1} indicated the presence of aromatic rings with C=C bonds. In addition, the absorption peak at 1446 cm^{-1} was attributed to the deformation of C–C bond within the phenolic moiety, while the absorption peak at 1321 cm^{-1} indicated the presence of phenolic groups. The absorption peak at 1197 cm^{-1} was attributed to the deformation of the C–H bond, while the vibrational bands at 1100–1000 cm^{-1} were attributed to the deformation of the C–O and C–H bonds. Our findings are consistent with those of previous reports in the literature.[35] Compared to TA, the Cu/TA nanozyme exhibited peak splitting and shifts in the FT-IR spectrum due to oxidation of TA and subsequent coordination with Cu^{2+}. Specifically, the peak of TA at 3347 cm^{-1} was split into three peaks at 3516 cm^{-1}, 3440 cm^{-1}, and 3355 cm^{-1}. This splitting phenomenon indicates that the coordination of TA with Cu^{2+} disrupted the phenolic hydroxyl HO–C vibration of TA.[33] Furthermore, there was a significant shift of the absorption peaks within the fingerprint region of the FT-IR spectrum of Cu/TA nanozyme, which serves as confirmation of the coordination of TA with Cu^{2+}.

In order to understand the oxidation state of Cu in Cu/TA nanozyme, it was further characterized by XPS. As shown in Fig. 2b, the full-scan spectrum of Cu/TA nanozyme demonstrated the presence of Cu, O and C elements, indicating that the product was an inorganic-organic hybrid. The high-resolution spectrum of Cu 2p displays peaks at 933.6 eV (Cu 2p3/2) and 954.0 eV (Cu 2p1/2), accompanied by characteristic shake-up satellite peaks at 940.8 eV and 961.0 eV, respectively (Fig. 2c).[36] The different valence states of Cu were distinguished using X-ray Auger spectra. As shown in Fig. 2d, the Cu LMM Auger spectrum was deconvoluted into Cu^{2+} and Cu^{+} peaks at 918.2 eV and 912.7 eV, respectively. These results indicate that Cu^{2+} combine with TA in a coordination form.

The morphology of Cu/TA nanozyme was observed using SEM (Fig. 3a). The prepared Cu/TA nanozyme exhibited two distinct morphologies. The larger structure exhibited a sheet-like morphology, with a diameter of approximately 280 nm and a thickness of approximately 31 nm. The smaller particle-like structure had a diameter of approximately 28 nm. These results are consistent with those reported in the literature.[33] The EDS elemental analysis of Cu/TA nanozyme was shown in

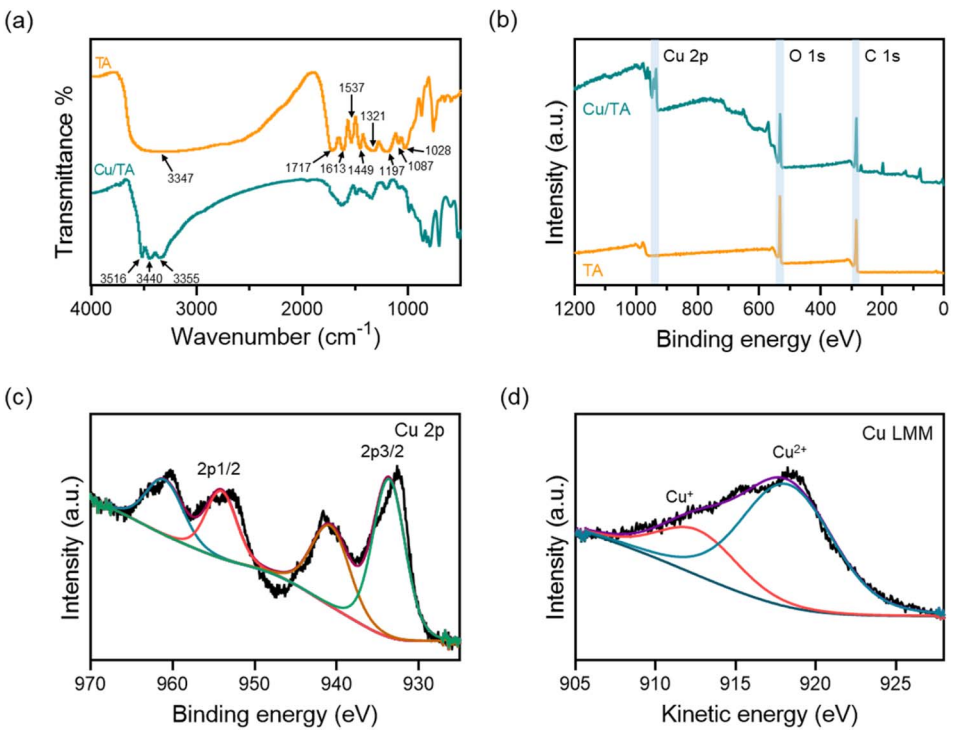

Fig. 2 (a) FT-IR spectra of TA and Cu/TA nanozyme. (b) XPS survey spectra of TA and Cu/TA nanozyme. (c) Cu 2p high-resolution spectra and (d) Cu LMM Auger spectra of Cu/TA nanozyme.

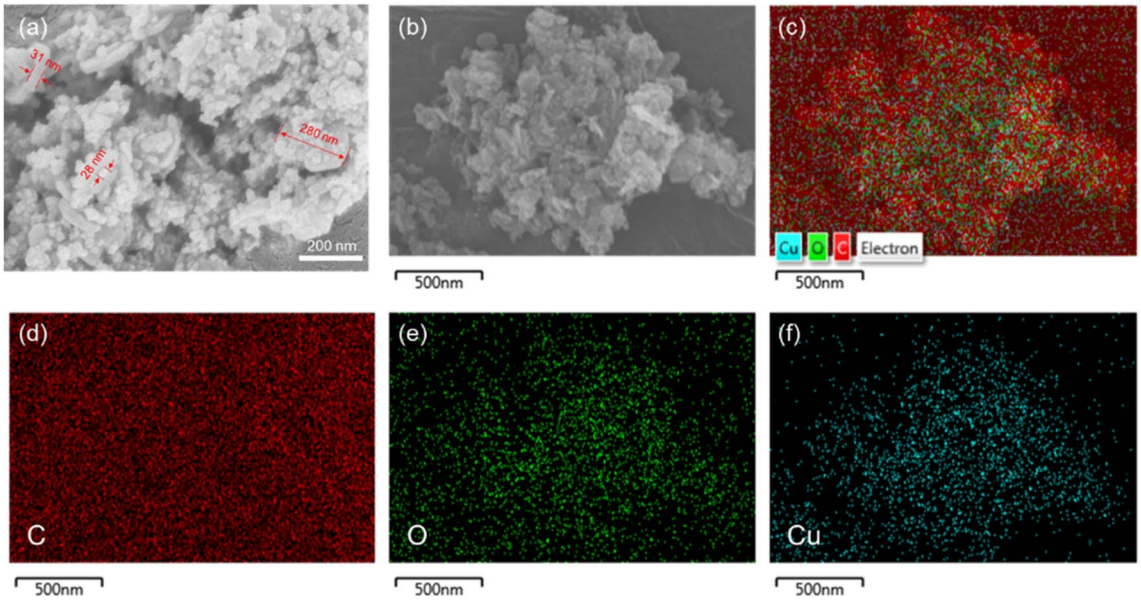

Fig. 3 (a) SEM image and (b–f) EDS elemental analysis of Cu/TA nanozyme.

Fig. 3b–f. The presence and uniform distribution of carbon, oxygen, and copper elements on Cu/TA nanozyme also confirms the successful synthesis.

The hydrodynamic size and zeta potential of Cu/TA nanozymes were measured by DLS (Fig. 4). As shown in Fig. 4a, the hydrodynamic size of Cu/TA nanozyme was determined to be approximately 503 nm, with a PDI of 0.396. The hydrodynamic particle size incorporates the solvent layer and thus exhibits a slight discrepancy from the actual particle size. As shown in Fig. 4b, the zeta potential of Cu/TA nanozyme was 13.3 mV, which was higher than that of pure TA at −17.7 mV. This shift can be attributed to the introduction of the positively charged Cu^{2+}, which neutralized the negatively charged phenolic hydroxyl groups of TA. The high absolute value of the zeta potential of Cu/TA nanozyme indicates that it has a stable structure and uniform dispersion in deionized water.

3.1.2 Thermal stability and multienzyme-like activity of Cu/TA nanozyme. The thermal stability of Cu/TA nanozyme was investigated using TGA (Fig. 5a). The mass loss below 100 °C usually originates from residual solvents.[37] The coordination between TA and Cu^{2+} significantly enhanced the thermal stability of Cu/TA nanozyme compared to TA.

The antioxidant capacity of the obtained Cu/TA nanozyme was confirmed by a series of free radical scavenging assays (Fig. 5b–d). The ability of Cu/TA nanozyme to scavenge $^{\bullet}O_2^-$ was first determined since it has a coordination active center similar to that of natural SOD. $^{\bullet}O_2^-$ is one of the most destructive reactive oxygen radicals,[38] and the ability of Cu/TA nanozyme to catalyze the decomposition of $^{\bullet}O_2^-$ was examined using the inhibition and produce superoxide anion assay kit. During the assay, $^{\bullet}O_2^-$ was generated by the reaction between xanthine and xanthine oxidase Following the addition of an electron transfer substance and Gress's reagent, the reaction system displayed a purple-red coloration and a characteristic absorption peak at 550 nm. As shown in Fig. 5b, the absorbance value of the solution at 550 nm was higher without Cu/TA nanozyme. Conversely, the presence of Cu/TA nanozyme resulted in the decomposition of $^{\bullet}O_2^-$, which led to a decrease in the

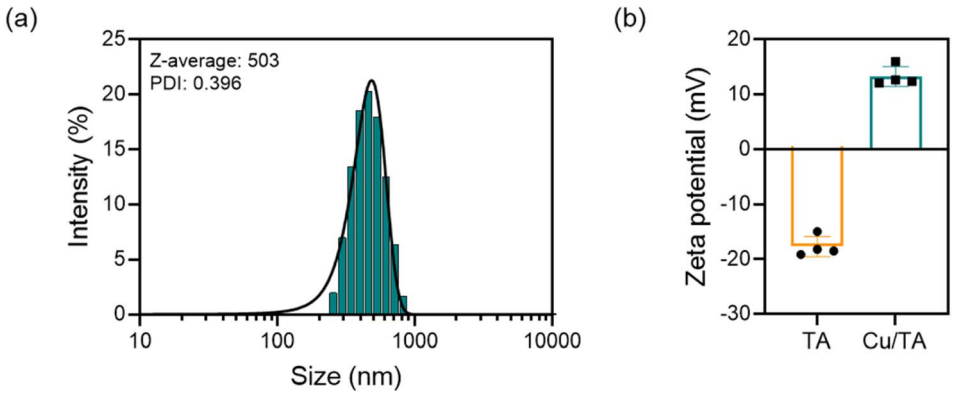

Fig. 4 (a) Hydrodynamic particle size distribution and (b) zeta potential of Cu/TA nanozyme.

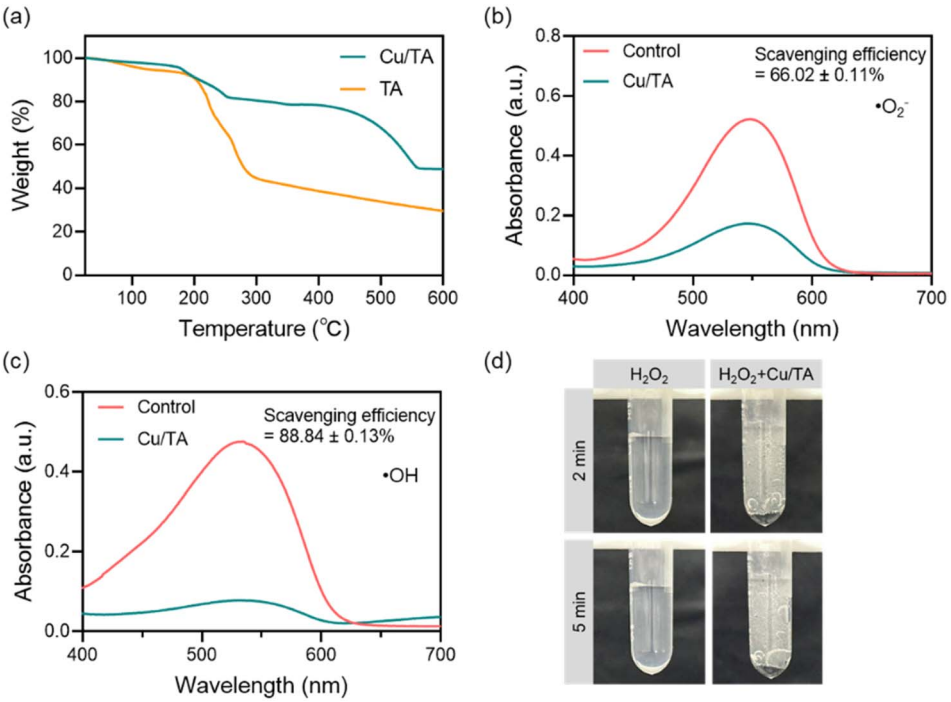

Fig. 5 (a) TGA curves of TA and Cu/TA nanozyme. (b) Absorption spectra of solutions after reaction with $^{\bullet}O_2^-$. (c) Absorption spectra of solutions after reaction with $^{\bullet}OH$. (d) Photographs of H_2O_2 decomposing to produce O_2 in 5 min in the absence and presence of Cu/TA nanozyme.

absorbance value of the solution. The Cu/TA nanozyme exhibited enhanced $^{\bullet}O_2^-$ scavenging ability compared to Cu^{2+} and pure TA (Fig. S1a†). The results indicate that the Cu/TA nanozyme exhibited SOD-like activity. pH is one of the important factors affecting the activity of nanozymes. We investigated the pH-dependent SOD-like activity of Cu/TA nanozyme. As shown in Fig. S2a in the ESI,† the optimal pH for SOD-mimicking Cu/TA nanozyme was 7.0, but it still maintained good SOD-like activity at pH 5.0 and 9.0, which could scavenge 63.7% and 61.6% of $^{\bullet}O_2^-$, respectively. As a result, Cu/TA nanozyme maintained high SOD-like activity over a wide pH range.

In addition, Cu/TA nanozyme also showed the ability to eliminate $^{\bullet}OH$. $^{\bullet}OH$ is a highly oxidizing reactive oxygen radical that can cause damage to cell membranes and DNA. Therefore, the removal of $^{\bullet}OH$ can have a positive effect on protecting cells or organisms more effectively from free radical-induced damage.[38] The hydroxyl free radical assay kit was employed to investigate the scavenging efficiency of Cu^{2+}, TA and Cu/TA nanozyme for $^{\bullet}OH$, which is generated by the classical Fe^{2+}/H_2O_2 Fenton reaction. As shown in Fig. 5c and S1b,† Cu/TA nanozyme can eliminate more than 80% of $^{\bullet}OH$, which was significantly higher than that of Cu^{2+} and TA, showing a high $^{\bullet}OH$ scavenging ability. In addition, Cu/TA nanozyme maintained a favorable $^{\bullet}OH$ scavenging ability in a broad pH range (Fig. S2b†).

H_2O_2 is another important reactive oxygen species with high oxidizing capacity, which is a downstream product of $^{\bullet}O_2^-$.[1] Catalase can catalyze the decomposition of H_2O_2 into H_2O and O_2.[5] As shown in Fig. 5d and S1c,† no bubbles were generated in the pure H_2O_2 solution and the solution with incorporated TA, whereas a large number of O_2 bubbles were generated after the addition of Cu/TA nanozyme. Thus, it can catalyze the decomposition of H_2O_2 to produce O_2, confirming that Cu/TA nanozyme has catalase-like activity. These results indicate that Cu/TA nanozyme is efficient in scavenging free radicals.

The POD-like activity of Cu/TA nanozyme was evaluated by oxidizing TMB to oxTMB.[39–41] As shown in Fig. S3,† in the presence of H_2O_2 substrate, Cu/TA nanozyme was capable of efficiently catalyzing the oxidation of TMB to produce blue oxTMB with characteristic absorption at 652 nm. In contrast, there was no significant absorbance signal in the presence of H_2O_2 or Cu/TA nanozyme alone. These results indicate that Cu/TA nanozyme also exhibits POD-like enzyme activity to catalyze the generation of $^{\bullet}OH$ from H_2O_2.

Considering the presence of multiple Cu valence states in Cu/TA nanozyme and the inherent antioxidant properties of TA, a possible mechanism for radical scavenging by Cu/TA nanosheets was proposed. Cu(I) can be oxidized to Cu(II) by $^{\bullet}O_2^-$ to produce H_2O_2.[42] The coordination structure of Cu(II) can be converted to Cu(I) by oxidizing $^{\bullet}O_2^-$ to produce O_2 molecules.[34] The valence state transition of Cu in Cu/TA is necessary for $^{\bullet}O_2^-$ disproportionation.[20,34] Cu/TA nanozyme can promote the electron transfer reaction, which inactivates $^{\bullet}OH$ or H_2O_2. The pronounced CAT-like enzyme activity of Cu/TA nanozyme may be related to the Cu(I) coordination structure, which catalyzes the decomposition of H_2O_2 into O_2 and H_2O. In addition, polyphenolic ligands can facilitate the catalytic process by performing valence conversion of Cu.[27,34] These results demonstrate the importance of Cu coordination with TA in determining its enzymatic activity.

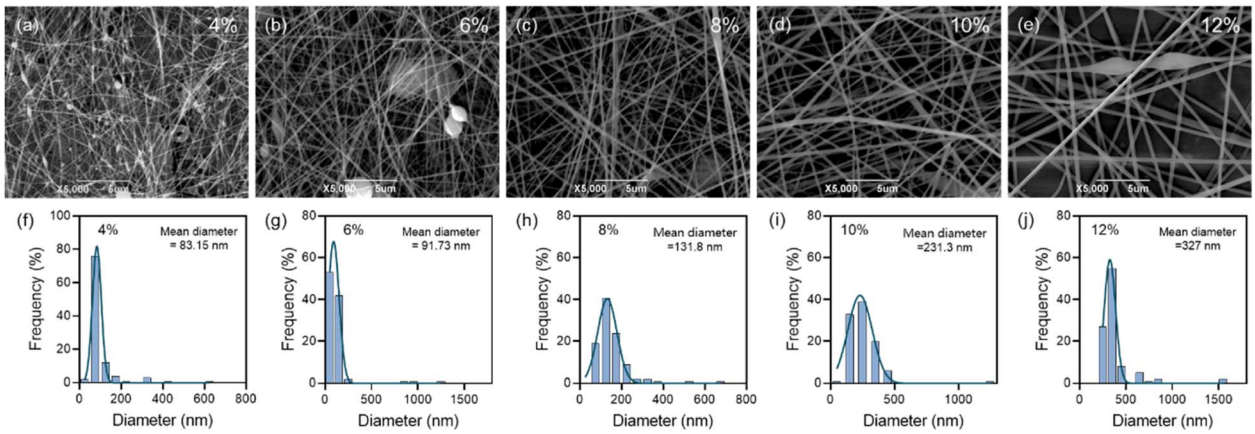

Fig. 6 (a–e) SEM images and (f–j) fiber diameter distribution of PAN nanofibrous membranes at various spinning solution concentrations.

3.2 Preparation and characterization of nanofibrous membranes

3.2.1 Effect of solution concentration on PAN membrane morphology. The surface morphology of the PAN nanofibrous membrane at different concentrations was observed by SEM. As shown in Fig. 6a–e, when the PAN concentration was low, the jet exhibited instability during the spraying process, resulting in the formation of sparse fibers and a prevalence of beaded structures. This phenomenon can be attributed to the fact that a lower concentration of PAN leads to a reduced degree of chain entanglement, resulting in a diminished viscosity and an inability to stabilize and stretch the jet under the influence of the electric field.[43] When the concentration of PAN was increased to 10 wt%, the spinning process was continuous without liquid dripping. The fibers formed had smooth surfaces, uniform sizes and no beading structure, indicating that the various external forces on the jet at this concentration were relatively balanced and could be sufficiently stretched and extended.[44] As the concentration of the PAN spinning solution increases, fiber sticking and spindle-like structures become more prevalent. This is mainly due to the elevated viscosity of the solution at high concentrations, which tends to induce the clogging of the needles, thereby resulting in discontinuous electrospinning.[45,46] Therefore, 10 wt% PAN solution was used for subsequent experiments.

3.2.2 Effect of flow rate on PAN membrane morphology. The flow rate of spinning solution has an important effect on the morphology of nanofibers.[47] As shown in Fig. 7, the SEM images of PAN nanofibrous membranes prepared at varying flow rates are presented. At a low flow rate (0.5 mL h^{-1}), it was difficult for the spinning solution to form a Taylor cone at the tip of the needle, which results in an unstable spinning jet and a lower spinning efficiency (Fig. 7a). At a high flow rate (1.5 mL h^{-1}), the solvent evaporation time was reduced, resulting in

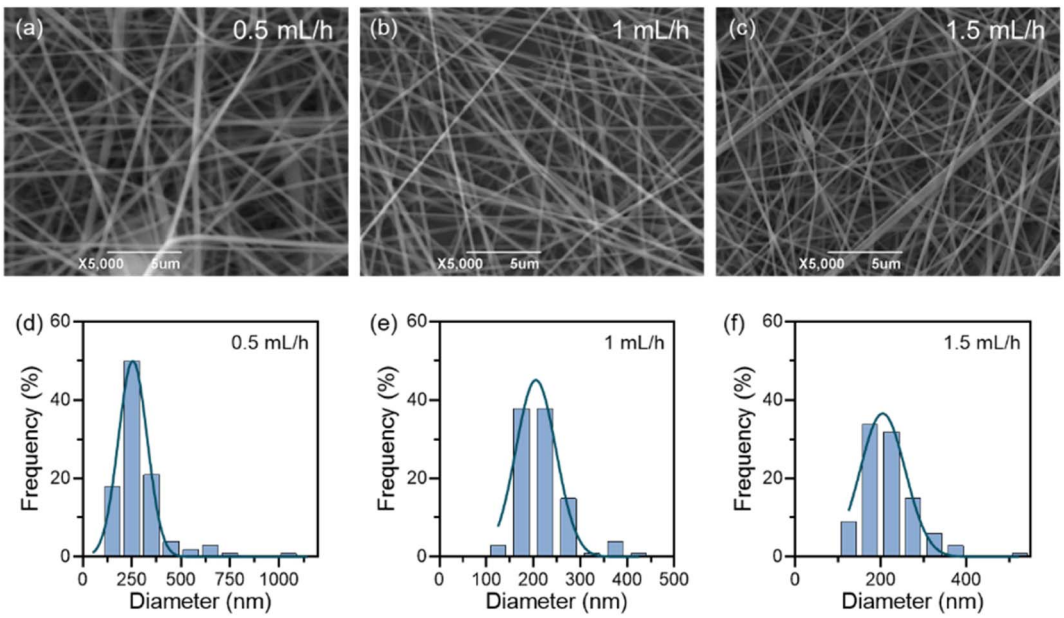

Fig. 7 (a–c) SEM images and (d–f) fiber diameter distribution of PAN nanofibrous membranes at various spinning flow rates.

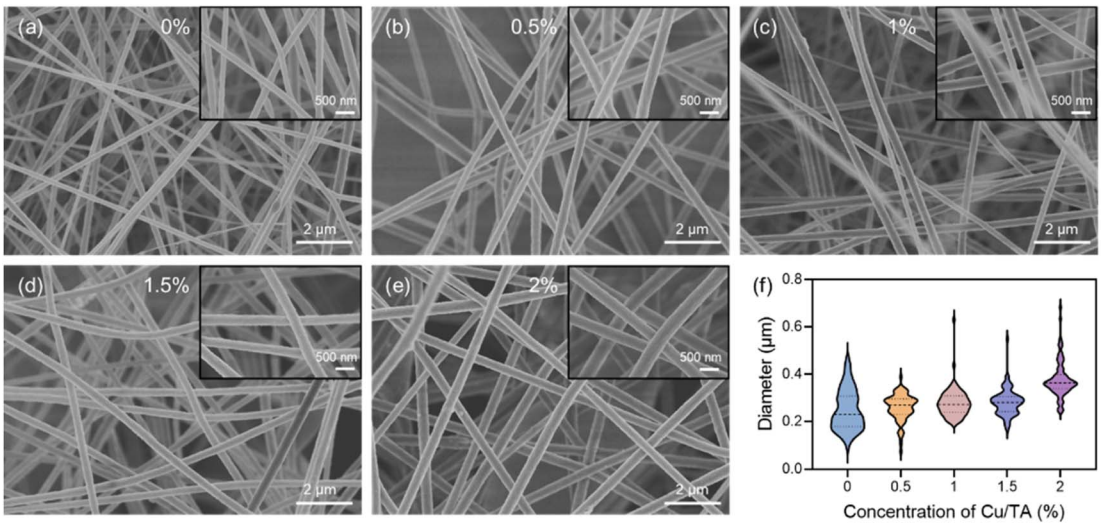

Fig. 8 (a–e) SEM images and (f) fiber diameter distribution of CTP membranes at various Cu/TA nanozyme concentrations.

incomplete evaporation. This led to the adhesion of fibers obtained on the receiving plate and the formation of flat and wide fibers.[48] At the same time, the spinning solution flow rate was excessive, thereby preventing the jet from being stretched effectively and resulting in the formation of a spindle-like structure (Fig. 7c).[49] Therefore, the optimal spinning flow rate for 10 wt% PAN solution was 1 mL h^{-1}.

3.2.3 Effect of Cu/TA nanozyme concentration on CTP membrane morphology. According to the optimized optimal process parameters, Cu/TA nanozyme was blended with PAN solution and subsequently subjected to electrospinning. As shown in Fig. S4,† the presence and uniform distribution of carbon, nitrogen, oxygen, and copper elements on the fibers confirmed the successful introduction of Cu/TA nanozyme into the CTP membrane. As shown in Fig. 8, the surface morphology and fiber diameter distribution of the nanofibrous membranes with different Cu/TA nanozyme concentrations are presented. In comparison to pure PAN nanofibers, the surface of the composite nanofibers became rough following the addition of Cu/TA nanozyme and small particle aggregations could be observed, indicating the successful loading of Cu/TA nanozyme (Fig. 8a–e). In addition, the diameter of the composite nanofibers increased significantly when the concentration of Cu/TA nanozyme was increased from 0 to 2% (Fig. 8f).

3.2.4 Antioxidant ability of CTP membranes. In view of the excellent free radical scavenging activity of Cu/TA nanozyme, the composite membranes loaded with Cu/TA nanozyme were tested for their antioxidant capacity. The antioxidant capacity of

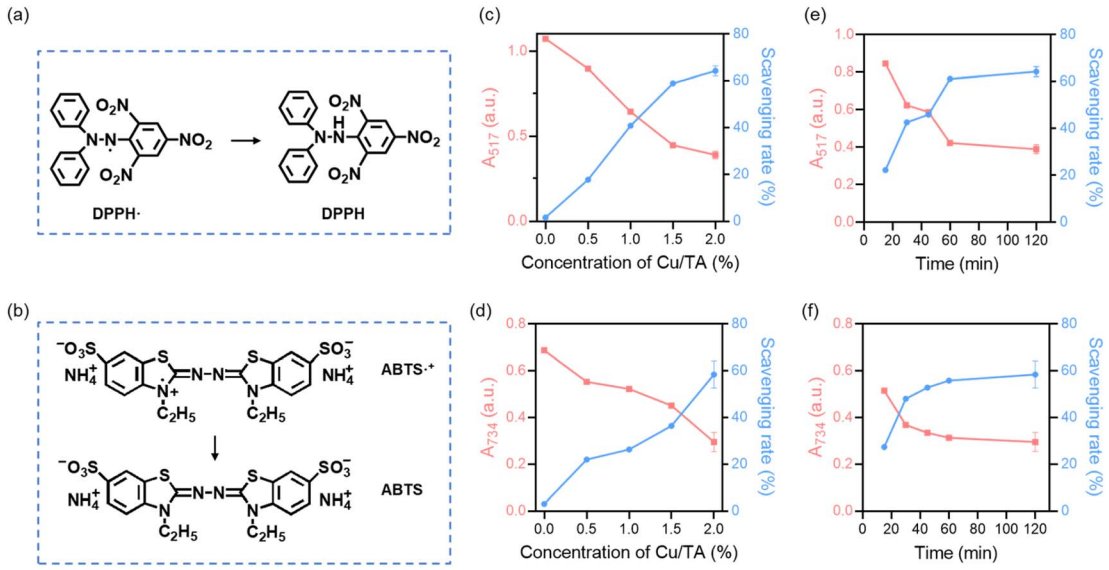

Fig. 9 Schematic of the reaction mechanism for scavenging (a) DPPH• and (b) ABTS•+. Scavenging rate of (c) DPPH• and (d) ABTS•+ by CTP membranes containing different concentrations of Cu/TA nanozymes. Scavenging rate of (e) DPPH• and (f) ABTS•+ by CTP membranes containing 2% Cu/TA nanozymes at different time points.

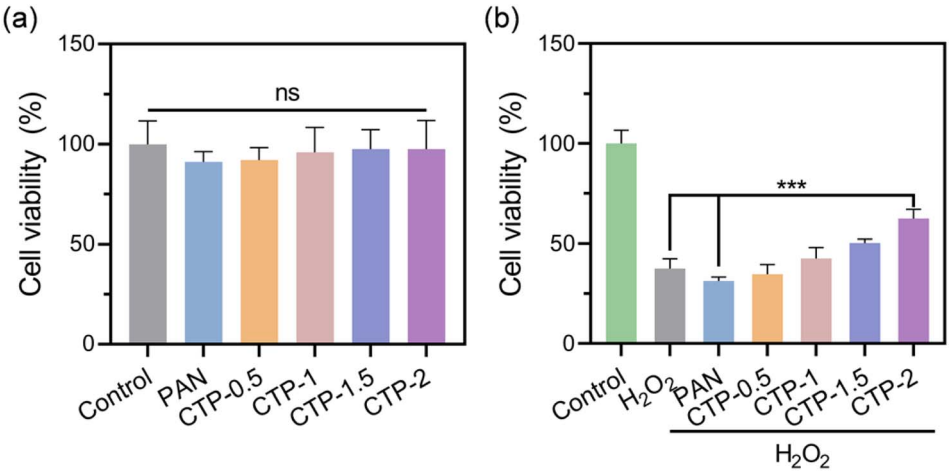

Fig. 10 (a) Cell viability obtained by treating L929 cells with different nanofiber membrane extracts. (b) Cell viability obtained by treating L929 cells with different nanofiber membranes in H_2O_2-containing environment.

different nanofibrous membranes was evaluated by DPPH and ABTS radical scavenging experiments. The reduction of DPPH$^{\bullet}$ and ABTS$^{\bullet+}$ was reported to involve hydrogen atom or electron transfer (Fig. 9a and b).[50] The results of the DPPH radical scavenging experiments showed that the composite membrane incorporating Cu/TA nanozyme had a lower absorbance value at 517 nm after reacting with DPPH$^{\bullet}$ solution compared to PAN membrane, suggesting that Cu/TA nanozyme conferred free radical scavenging ability to the PAN membrane in a concentration-dependent manner (Fig. 9c). In addition, the DPPH radical scavenging rate of CTP membranes with 2% Cu/TA nanozyme content demonstrated an increase in scavenging efficiency over time following the reaction with DPPH ethanol solution in the absence of light for 15, 30, 45, 60, and 120 min. The scavenging efficiency of DPPH$^{\bullet}$ reached a maximum of 64.22% at 120 min (Fig. 9e). Similarly, the scavenging ability of different nanofibrous membranes against ABTS radicals was examined. The results showed that the scavenging ability of the CTP membrane for ABTS$^{\bullet+}$ was also concentration-dependent and time-dependent, with the highest scavenging efficiency up to 58.44% (Fig. 9d and f).

3.2.5 Cytocompatibility and effect on cell survival in ROS microenvironment of CTP membranes. To verify the cytocompatibility of CTP membranes, the L929 cells were cultured with different extracts of nanofiber membranes, and the cell viability of different samples was analyzed. The cells incubated with untreated DMEM were utilized as the control group. As shown in Fig. 10a, the cell viability of cells incubated with different membrane extracts was not significantly different from that of the control group, demonstrating that the CTP membranes do not exhibit cytotoxicity.

In order to simulate the *in vitro* ROS microenvironment, 500 μM H_2O_2 was used to induce oxidative stress. The L929 cells were cultured in the artificial oxidative stress environment for 6 h, and the cell viability was significantly reduced to 37% (Fig. 10b). Compared with PAN membranes, CTP membranes could significantly improve the viability of L929 cells in the H_2O_2-containing microenvironment, and the cell viability increased with the increase of Cu/TA nanozyme content in the nanofiber membranes. When the addition of Cu/TA nanozyme was 2%, the cell viability was reached up to 62%. The experimental results indicated that Cu/TA nanozyme in CTP membranes plays a key role in scavenging ROS and reducing cellular oxidative stress damage.

4 Conclusion

In summary, Cu/TA nanozymes constructed by self-assembly of Cu^{2+} and TA exhibited inherent SOD-like activity, catalase-like activity, and $^{\bullet}OH$ scavenging ability. These unique properties enable the Cu/TA nanozyme to effectively scavenge various free radicals. The Cu/TA nanozyme hybrid nanofibrous membranes were further made by electrospinning technique, and the results showed that the diameter of the composite fibers increased significantly after the introduction of Cu/TA nanozyme into the PAN fibers. In addition, the CTP composite membranes possessed excellent antioxidant capacity and were able to protect cells from oxidative stress damage. These results demonstrate the broad prospects of Cu^{2+}/TA self-assembled metal nanozymes in artificial enzyme development and open new avenues for the development of novel antioxidant films.

Data availability

All data generated or analyzed during this study are included in this published article. The data supporting this article have been included in the main article and the ESI.†

Author contributions

Qiao Wu: conceptualization, methodology, data curation, investigation, formal analysis, writing – original draft. Jingshu Xiao: methodology, investigation, software. Hu Zhuang: investigation, software. Fenghai Zhao & Ruoxi Li: methodology. Duntie Zhang: writing – review & editing, supervision, resources.

Conflicts of interest

The authors declare that they have no conflict of interest.

Acknowledgements

The authors would like to thank the School of Life and Health Sciences of Hubei University of Technology for providing instruments and services.

References

1 K. B. Beckman and B. N. Ames, *Physiol. Rev.*, 1998, **78**, 547–581.
2 X.-Q. Wang, W. Wang, M. Peng and X.-Z. Zhang, *Biomaterials*, 2021, **266**, 120474.
3 E. Cadenas, *Mol. Aspects Med.*, 2004, **25**, 17–26.
4 M. L. Circu and T. Y. Aw, *Free Radicals Biol. Med.*, 2010, **48**, 749–762.
5 J. Zhao, F. Guo, L. Hou, Y. Zhao and P. Sun, *J. Controlled Release*, 2023, **355**, 273–291.
6 Y. F. Mustafa, *Indian J. Clin. Biochem.*, 2024, **39**, 154–167.
7 S. Prasad, S. C. Gupta and A. K. Tyagi, *Cancer Lett.*, 2017, **387**, 95–105.
8 U. S. Srinivas, B. W. Q. Tan, B. A. Vellayappan and A. D. Jeyasekharan, *Redox Biol.*, 2019, **25**, 101084.
9 E. R. Stadtman and B. S. Berlett, *Drug Metab. Rev.*, 1998, **30**, 225–243.
10 C. Zhang, X. Wang, J. Du, Z. Gu and Y. Zhao, *Advanced Science*, 2021, **8**, 2002797.
11 S. Liang, X. Tian and C. Wang, *J. Inflammation Res.*, 2022, **15**, 6307–6328.
12 B. Halliwell, *Nat. Rev. Mol. Cell Biol.*, 2024, **25**, 13–33.
13 J. Liu, X. Han, T. Zhang, K. Tian, Z. Li and F. Luo, *J. Hematol. Oncol.*, 2023, **16**, 116.
14 A. Augustyniak, G. Bartosz, A. Čipak, G. Duburs, L. U. Horáková, W. Łuczaj, M. Majekova, A. D. Odysseos, L. Rackova, E. Skrzydlewska, M. Stefek, M. Štrosová, G. Tirzitis, P. R. Venskutonis, J. Viskupicova, P. S. Vraka and N. Žarković, *Free Radical Res.*, 2010, **44**, 1216–1262.
15 H. J. Forman and H. Zhang, *Nat. Rev. Drug Discovery*, 2021, **20**, 689–709.
16 D. Genovese, A. Baschieri, D. Vona, R. E. Baboi, F. Mollica, L. Prodi, R. Amorati and N. Zaccheroni, *ACS Appl. Mater. Interfaces*, 2021, **13**, 31996–32004.
17 P. Ghezzi, *Redox Biol.*, 2021, **44**, 102001.
18 M. Stoia and S. Oancea, *Antioxidants*, 2022, **11**, 638.
19 S. Zhou, H. Cai, X. He, Z. Tang and S. Lu, *Coord. Chem. Rev.*, 2024, **500**, 215536.
20 S. Lin, Y. Cheng, H. Zhang, X. Wang, Y. Zhang, Y. Zhang, L. Miao, X. Zhao and H. Wei, *Small*, 2020, **16**, 1902123.
21 Y. Huang, J. Ren and X. Qu, *Chem. Rev.*, 2019, **119**, 4357–4412.
22 X. Yu, Y. Wang, J. Zhang, J. Liu, A. Wang and L. Ding, *Adv. Healthcare Mater.*, 2024, **13**, 2302023.
23 Y. Tang, Y. Han, J. Zhao, Y. Lv, C. Fan, L. Zheng, Z. Zhang, Z. Liu, C. Li and Y. Lin, *Nano-Micro Lett.*, 2023, **15**, 112.
24 H. Jafari, P. Ghaffari-Bohlouli, S. V. Niknezhad, A. Abedi, Z. Izadifar, R. Mohammadinejad, R. S. Varma and A. Shavandi, *J. Mater. Chem. B*, 2022, **10**, 5873–5912.
25 W. Zhang, S. Roy, P. Ezati, D.-P. Yang and J.-W. Rhim, *Trends Food Sci. Technol.*, 2023, **136**, 11–23.
26 Z. Guo, W. Xie, J. Lu, X. Guo, J. Xu, W. Xu, Y. Chi, N. Takuya, H. Wu and L. Zhao, *J. Mater. Chem. B*, 2021, **9**, 4098–4110.
27 Y. Chen, X. Yang, K. Li, J. Feng, X. Liu, Y. Li, K. Yang, J. Li and S. Ge, *ACS Nano*, 2024, **18**, 7024–7036.
28 D. Li, J. Li, S. Wang, Q. Wang and W. Teng, *Adv. Healthcare Mater.*, 2023, **12**, 2203063.
29 Y. Huang, Y. Chen, G. Cheng, W. Li, H. Zhang, C. Yu, J. Fang, J. Zuo, Y. Li, L. Xu and D. Sun, *Int. J. Nanomed.*, 2024, **19**, 231–245.
30 Y. Xu, Y. Luo, Z. Weng, H. Xu, W. Zhang, Q. Li, H. Liu, L. Liu, Y. Wang, X. Liu, L. Liao and X. Wang, *ACS Nano*, 2023, **17**, 18732–18746.
31 V. Venezia, C. Prieto, M. Verrillo, M. Grumi, B. Silvestri, G. Vitiello, G. Luciani and J. M. Lagaron, *Int. J. Biol. Macromol.*, 2024, **263**, 130210.
32 S. Tie, Q. Zhang, Y. Zhao, Y. Wu, D. Liu, L. Zhao and S. Gu, *RSC Adv.*, 2024, **14**, 7572–7581.
33 Y. Wang, X. Wang, J. Wang, P. Zeng, P. Yang and A. Zhao, *Mater. Today Commun.*, 2024, **38**, 108130.
34 M. Wen, T. Wang, N. Li, Y. Wu, L. Zhang, Y. Xue and L. Shang, *Adv. Funct. Mater.*, 2024, 2403634.
35 B. Muhoza, S. Xia and X. Zhang, *Food Hydrocolloids*, 2019, **97**, 105174.
36 Y. Huang, H. Zhong, C. Jiang, J. Yang, J. Zhang, F. Zhao and C. Liu, *Particuology*, 2024, **84**, 126–135.
37 Z. Guo, R. Shen, Y. Chen, Y. Huo, J. Li, L. Zhou and J. Hu, *Adv. Funct. Mater.*, 2024, 2402633.
38 F. Xu, Y. Tang, H. Wang, H. Deng, Y. Huang, C. Fan, J. Zhao, C. Lin and Y. Lin, *Small*, 2022, **18**, 2201205.
39 F. Zhu, Y. Yu, Z. Yu, H. Qiu, G.-P. Lu, Z. Chen, J. Hu and Y. Lin, *Small*, 2024, **20**, 2311848.
40 Q. Fu, N. Wang, C. Zhou and X. Su, *Talanta*, 2024, **266**, 124991.
41 F. Mo, S. Zhong, T. You, J. Lu and D. Sun, *ACS Appl. Mater. Interfaces*, 2023, **15**, 52114–52127.
42 T. Liu, B. Xiao, F. Xiang, J. Tan, Z. Chen, X. Zhang, C. Wu, Z. Mao, G. Luo, X. Chen and J. Deng, *Nat. Commun.*, 2020, **11**, 2788.
43 S. Luo, A. Saadi, K. Fu, M. Taxipalati and L. Deng, *J. Sci. Food Agric.*, 2021, **101**, 6355–6367.
44 J. Xi, S. Shahab and R. Mirzaeifar, *RSC Adv.*, 2022, **12**, 29162–29169.
45 H. Salimi-Kenari, M. Barari, S. R. Nabavi, A. Mousavi Anjeh and S. R. Hosseini, *Polym.-Plast. Technol. Mater.*, 2023, **62**, 294–305.
46 H. Gade, S. Nikam, G. G. Chase and D. H. Reneker, *Polymer*, 2021, **228**, 123902.

47 Z. Sun, M. Li, Z. Jin, Y. Gong, Q. An, X. Tuo and J. Guo, *Int. J. Biol. Macromol.*, 2018, **120**, 2552–2559.
48 A. Refate, Y. Mohamed, M. Mohamed, M. Sobhy, K. Samhy, O. Khaled, K. Eidaroos, H. Batikh, E. El-Kashif, S. El-Khatib and S. Mehanny, *Heliyon*, 2023, **9**, e17051.
49 W. Zuo, M. Zhu, W. Yang, H. Yu, Y. Chen and Y. Zhang, *Polym. Eng. Sci.*, 2005, **45**, 704–709.
50 İ. Gulcin, *Arch. Toxicol.*, 2020, **94**, 651–715.